Mg-Doped $CdTeO_3$ Quantum Dot Sensitized Solar Cells

Yuanyuan Li[1, a], Xiaoping Zou[2, b], and Chuan Zhao[3, c]

Research Center for Sensor Technology, Beijing Key Laboratory for Sensor, Ministry of Education Key Laboratory for Modern Measurement and Control Technology, School of Applied Sciences, Beijing Information Science and Technology University,

Jianxiangqiao Campus, Beijing 100101, China

[a]aimee_yuan2015@sina.com, [b]xpzou2014@163.com, [c]zhaochuancn@sina.com

Keywords: Solar cell, p-type, doping

Abstract. To study the influence of doping on p-type solar cells, we use the p-type NiO/$CdTeO_3$ structure to fabricate Mg-doped $CdTeO_3$ quantum dot-sensitized solar cells (QDSSCs), by doping $CdTeO_3$-sensitized NiO photocathode with dopant element Mg. When the doping ratio of Mg is 1:30 and the successive ionic layer adsorption and reaction (SILAR) cycles are 2, we get the short-circuit current density of 0.387 mA/cm^2, which is obviously higher than that (0.348 mA/cm^2) of the undoped ones. Here in this report, we emphatically analyzed the effect of doping ratio and SILAR cycles on the properties of QDSSCs. And it is an important attempt on the development of p-type NiO/$CdTeO_3$ QDSSCs.

Introduction

Quantum dots-sensitized solar cells have been widely researched and show promise toward the development of next generation of energy, due to the characteristics of low cost, environmental protection and high theoretical power conversion efficiency [1-3]. What's more, the quantum dots (QDs) also have lots of characteristics that make QDSSCs popular, such as high absorption coefficient, tunable band gap, and multiple exciton generation (MEG) effect [4-7]. However, the real photoelectric conversion efficiency is still low due to many factors, among which the carrier recombination with redox couple on the semiconductor interface and a low rate of hole transport are most commonly encountered. Recent studies have pointed out that the efficiency of tandem DSSCs is higher than that of the single n-type DSSCs or p-type DSSCs [8]. As we all know, the photocurrent density of n-type solar cell is much higher than that of p-type solar cell, and the current of tandem solar cell is decided by the lower current of n-type and p-type cells. Therefore, improving the performance (especially the short-circuit current density) of p-type solar cell is conducive to realizing high theoretical power conversion efficiency of QDSSCs [9].

In 2009, for the first time, Rhee et al. deposited sensitizer Cu_2S on mesoporous NiO electrode to fabricate p-type NiO/Cu_2S solar cell, which set a precedent for quantum dots deposition on p-type NiO film, and obtained the short-circuit current density of 0.260-0.360 mA/cm^2, open circuit voltage of 91-95 mV [10]. In 2011, Soon Hyung Kang et al. sensitized NiO with CdS, and achieved a short-circuit current density of 0.380 mA/cm^2, open circuit voltage of 350 mV and the conversion efficiency of 0.027% [11]. In addition, in 2014, Chuan Zhao and some other members of our laboratory assembled the p-type NiO/$CdTeO_3$ structure, and obtained a photovoltage of 103.7 mV and a short-circuit current density of 0.364 mA/cm^2 [12].

In this paper, firstly we regulated the properties of QDs by doping element Mg into the precursor solution of $CdTeO_3$ to improve cell performance. Then the Mg-doped $CdTeO_3$ QDs were deposited onto NiO mesoporous substrate by SILAR method. At last, the Mg-$CdTeO_3$ QDs-sensitized NiO film was used as the photocathode in the thin sandwich-type cell with counter electrode Pt-coated FTO, spacer, and electrolyte. By contrast, the power conversion efficiency (0.016 %) under air mass (AM) 1.5 condition (100 mW/cm^2), is almost the same as that (0.016%) of undoped ones, but the short-circuit current density (0.387 mA/cm^2) has a huge improvement in our experiment, which has an important effect on the realization of tandem DSSCs of n-type and p-type DSSCs with a higher current density.

Materials and Methods

NiO paste was made by rotary evaporation method [13] which removed ethanol from the mixed material, which includes 15 g NiO nanopowder in ethanol, 50mL 10 wt% ethanolic ethyl cellulose solution and 100 mL terpineol. Then the NiO nanoparticles were uniformly coated on the surface of the FTO (fluorine-doped tin oxide) by screen printing method, followed by annealing it at 450 °C for 30 min. The thickness of the film is controlled by the number of screen print. Here, I screen printed two layers of NiO, by annealing it at 125 °C for 5 min after the first print and then sintering it at 450°C for 30 min after the second print. And the counter electrode is coated with Pt which is obtained from the thermal decomposition of chloroplatinic acid [14]. The working area of the solar cell was 0.5×0.5 cm^2.

Here in this work, the electrolyte was prepared by dissolving 1.0 M LiI and 0.1 M I_2 into acetonitrile [15]. And the Mg-doped $CdTeO_3$ QDs were deposited on NiO substrate by SILAR method. Dopant $MgCl_2$ was dissolved into $Cd(NO_3)_2$ ethanol solution (0.01 M) as the precursor solution of cation, according to different doping concentration. The Na_2TeO_3 aqueous solution (0.01 M) was as the anion source. The prepared NiO photocathode was firstly immersed in the mixed ethanol solution of $Cd(NO_3)_2$ and $MgCl_2$ for 5 min, followed by rinsing with ethanol and drying with nitrogen. Subsequently, the NiO photocathode was dipped into Na_2TeO_3 aqueous solution (0.01 M) for another 5 min at 30°C, and rinsed again with deionized water, dried with nitrogen. Then, one cycle of SILAR has been completed.

Results and Discussion

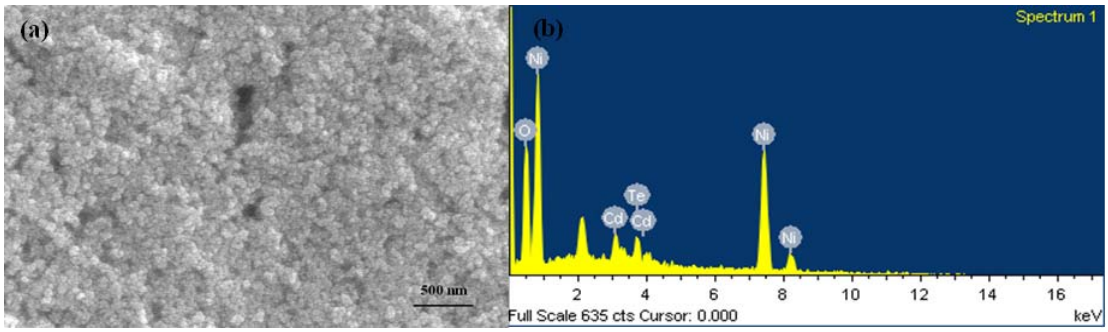

Fig. 1: (a) SEM image of Mg-doped-$CdTeO_3$ sensitized NiO photocathode and (b) the corresponding EDS spectrum.

Fig. 1(a) shows the scanning electron micrograph (SEM) of the NiO film deposited by Mg-doped-$CdTeO_3$ QDs, which is composed of nanoparticles with relatively uniform distribution, but the Mg-doped QDs cannot be found in it. Fig. 1(b) is the corresponding EDS spectrum, and from it, we can find O, Ni, Cd, and Te elements, but can't find the Mg element, which is because the Mg doping ratio is so low that the instrument can't detect.

In order to determine the content of element Mg and Cd, we take the ICP-MS test for the samples and the result is shown in Table 1. Through the analysis of Table 1 and by converting them to mole ratio, we get the real molar ratio of element Mg and Cd (0.45%), which is far less than the designed molar ration (1:30). Furthermore, the XRD patterns of NiO film deposited with $CdTeO_3$ QDs (Fig. 2) is quoted here to clearly analyze material composition, due to that the same method is used to carry out the experiment. The typical X-ray diffraction pattern peaks at 2θ values of NiO film are approximately 37.4°, 43.3°, and 62.9°, which correspond to (111), (200), and (220) crystalline planes, respectively. And the X-ray diffraction patterns of FTO, NiO, and $CdTeO_3$ can be found from it. The typical X-ray diffraction pattern peaks at 2θ values of $CdTeO_3$ QDs are approximately 28.8° and 33.1°, which correspond to (111) and (200) crystalline planes of $CdTeO_3$, respectively [12].

Table 1: ICP-MS quantitative analysis of Mg-doped-$CdTeO_3$ QDSSCs.

Sample	Mg mass ration (%)	Cd mass ration (%)
1:30 Mg-$CdTeO_3$	0.0039	4.009

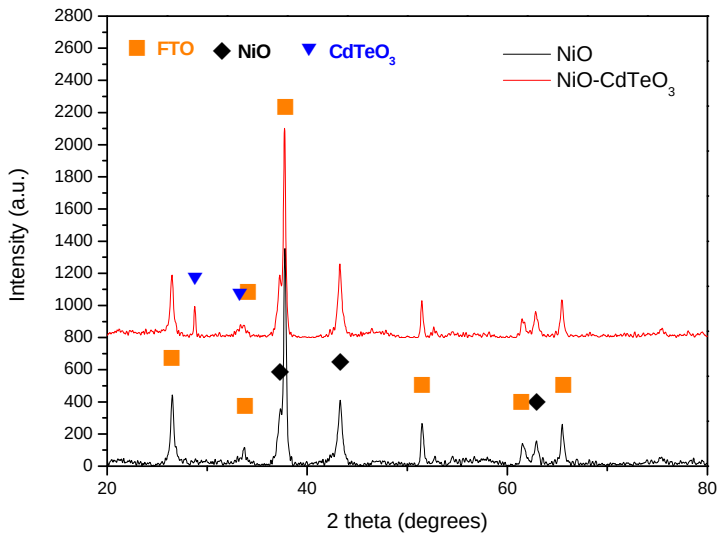

Fig. 2: XRD patterns of the NiO mesoporous film deposited with $CdTeO_3$ QDs

The J-V characteristic curves of Mg-doped $CdTeO_3$ QDSSCs with different doping ratio is shown in Fig. 3, and the SILAR cycles are fixed on 4. Simultaneously, the corresponding performance parameters are presented in Table 2. From J-V curves, we can find that the open circuit voltage (Voc) decreases after doping element Mg, and it suggests that Mg-doping has caused the Fermi level of QDs sensitized NiO photocathode rise, leading to the difference value (V_{OC}) between the Fermi level of photocathode and redox potential of the electrolyte decrease, as is shown in Fig. 4. When the Mg doping concentration is 1:30, the power conversion efficiency reaches to the maximum value (0.016%). And the short-circuit current density (Jsc) of Mg-doped-$CdTeO_3$ QDSSCs is 0.387 mA/cm^2, obviously higher than that of undoped $CdTeO_3$ QDSSCs (0.348 mA/cm^2), which demonstrates that when the doping ratio is 1:30, Mg-doping has a significant effect on current promotion.

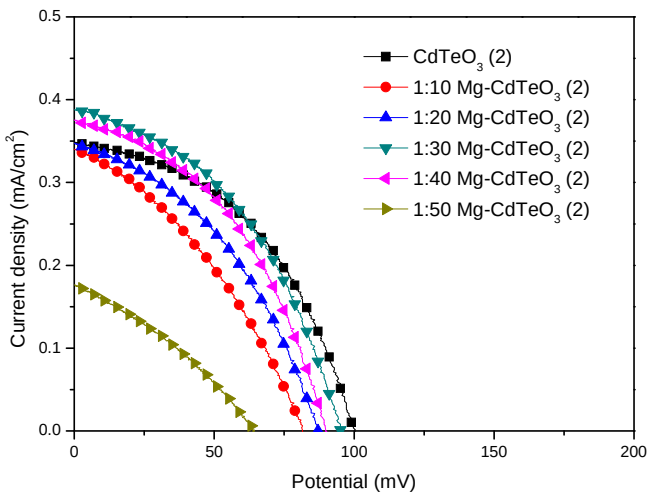

Fig. 3: *J-V* characteristic curves of Mg-doped-$CdTeO_3$ QDSSCs with different doping ratio

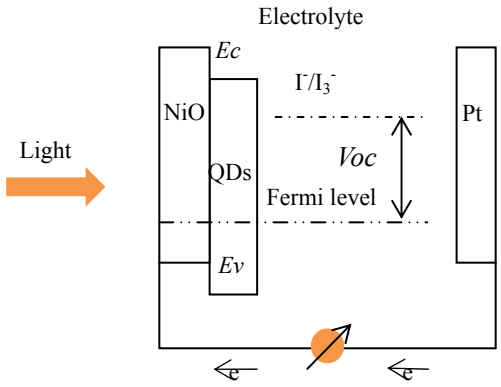

Fig. 4: The structure and energy level of Mg-doped-$CdTeO_3$ QDSSCs

By comparing the experiment results with different doping proportion, we can find that with the decrease of doping concentration, both the Jsc and the photoelectric conversion efficiency (η) are enhanced first and then get down. This is because when the doping concentration is relatively high, element Mg as the dopant in $CdTeO_3$ QDs, introduces much compound center, and the hole can't be transported to the FTO conductive glass effectively, which makes the Jsc decrease, and eventually reduces the η. When the doping concentration is 1:30, the promotion effect on Jsc of dopant Mg makes up for the impair of impurity recombination center to it, so the comprehensive performance of Jsc has been greatly improved. When doping concentration is small, the effect of impurity recombination center still exists, and is stronger than the promotion effect, so the Jsc gradually declines, and eventually leads to the decrease of the photoelectric conversion efficiency.

Table 2: Different photovoltaic parameters for different doping ratios.

Samples	V_{oc} (mV)	J_{sc} (mA/cm^2)	FF	η（%）
$CdTeO_3$ (2)	100.0	0.348	0.457	0.016
1:10 Mg-$CdTeO_3$ (2)	82.2	0.341	0.357	0.010
1:20 Mg-$CdTeO_3$ (2)	87.1	0.347	0.407	0.012
1:30 Mg-$CdTeO_3$ (2)	95.1	0.387	0.435	0.016
1:40 Mg-$CdTeO_3$ (2)	90.0	0.374	0.434	0.015
1:50 Mg-$CdTeO_3$ (2)	63.8	0.176	0.330	0.004

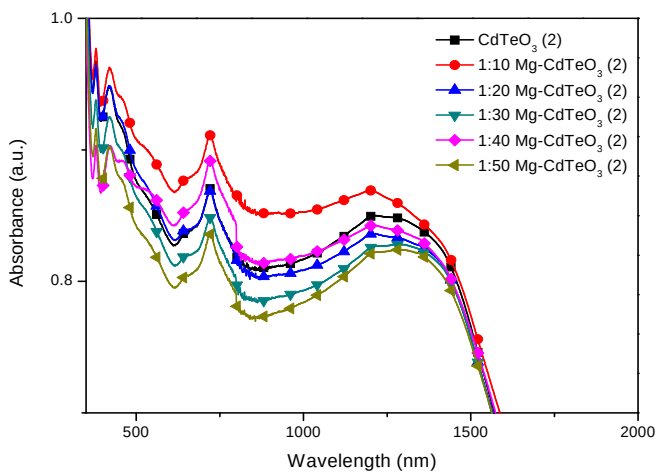

Fig. 5: Ultraviolet-visible-near infrared (UV-Vis) absorption spectra of undoped $CdTeO_3$ QDs and Mg-doped-$CdTeO_3$ QDs anchored on nanostructured NiO films with different doping ratio

Fig. 5 gives the UV-Vis absorption spectra of $CdTeO_3$ QDs and Mg-doped-$CdTeO_3$ QDs with different doping ratio. And we intercept the spectral wavelength range from 350 to 1500 nm. Obviously, the curve changes according to the same rule. There appear two small absorption peaks around 400 nm and 700 nm respectively. From the view of absorption intensity, it can be found that there is no obvious change with the variation of doping ratio. When the doping concentration is 1:10, the spectral absorption intensity of photocathode is the highest, and the lowest is with the doping concentration of 1:50. Thus we conclude that Mg doping can improve the spectral absorption intensity with proper doping ratio, and it may improve the Jsc indirectly, which is proportional to the product of the charge-collection efficiency and the light-harvesting efficiency.

In order to optimize the experimental condition, next we will research the influence of SILAR cycles on Mg-doped-$CdTeO_3$ QDSSCs.

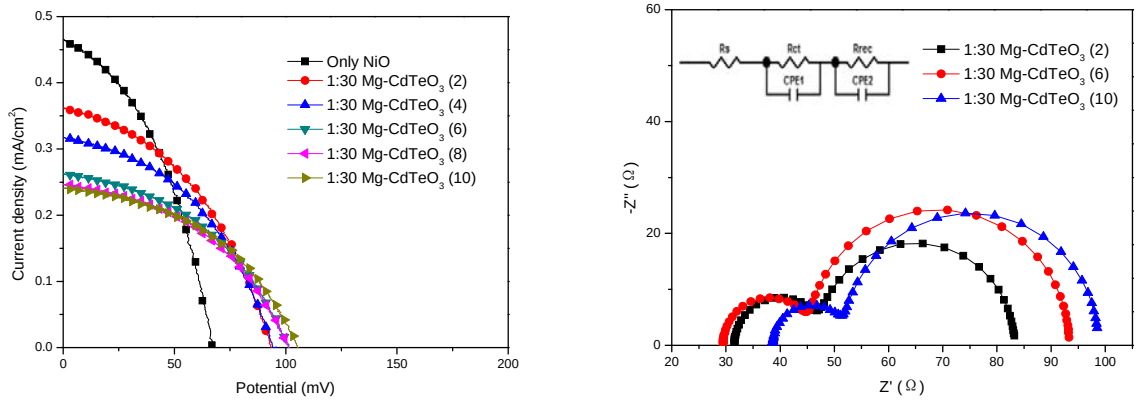

Fig. 6: J-V characteristic curves (right) and EIS (left) of Mg-doped-$CdTeO_3$ QDSSCs for different SILAR cycles with fixed doping ratio (1:30)

Table 3: Different photovoltaic parameters for different SILAR cycles

Samples	Voc (mV)	Jsc (mA/cm^2)	FF	η（%）
Only NiO	67.5	0.465	0.411	0.013
1:30 Mg-$CdTeO_3$ (2)	93.9	0.361	0.422	0.014
1:30 Mg-$CdTeO_3$ (4)	93.9	0.317	0.437	0.013
1:30 Mg-$CdTeO_3$ (6)	101.5	0.262	0.436	0.012
1:30 Mg-$CdTeO_3$ (8)	100.6	0.246	0.444	0.011
1:30 Mg-$CdTeO_3$ (10)	105.2	0.241	0.450	0.011

Table 4: The fitting parameters of EIS

Samples	R_s (Ω)	R_{ct} (Ω)	CPE1 (μF)	R_{rec} (Ω)	CPE2 (μF)
1:30 Mg-$CdTeO_3$ (2)	31.56	15.71	4.3	35.97	104.7
1:30 Mg-$CdTeO_3$ (6)	29.46	48.12	123.4	15.78	4.596
1:30 Mg-$CdTeO_3$ (10)	38.63	13.15	7.519	46.94	177.6

The J-V characteristic curves and corresponding performance parameters of Mg-doped-$CdTeO_3$ QDSSCs are presented in Fig. 6 (right) and Table 3. Obviously, with the increase of SILAR cycles (except when there are 10 cycles of SILAR and only NiO films), values of the Jsc and η of Mg-$CdTeO_3$-sensitized solar cells decrease. However, the fill factor (FF) keeps increasing with the repetition of SILAR cycles for nearly all the samples. When the SILAR cycles are 2, the conversion efficiency is 0.0143%. It is the highest efficiency that the Mg-doped-$CdTeO_3$ QDSSCs could achieve in terms of performance, with the corresponding Jsc is 0.361 mA/cm^2, and the Voc is 93.9 mV. With the increase of SILAR cycles, excessive accumulation of QDs leads to the bad coverage

and the interspace stoppage of mesoscopic NiO film, which is difficult for electrolyte to cover the surface of NiO film, thus the electrolyte cannot contact completely with Mg-$CdTeO_3$ QDs which are deposited on the surface of NiO film. In addition, along the thickness direction of deposited QDs, with the repetition of SILAR, there are introduced more interfaces that the carrier has to transfer, which increases the recombination probability of photo-generated holes and electrons, so both the Jsc and the photoelectric conversion efficiency decrease [16]. By contrast, with SILAR cycles increasing, the Voc gradually increases. This is because the accumulation of $CdTeO_3$ QDs may cause the Fermi level of Mg-$CdTeO_3$ QDs-sensitized NiO photocathode gradually move down, which leads to the different value between quasi-Fermi level of NiO and the redox potential of electrolyte increase. Thus with the repetition of SILAR, the Voc represents an increasing trend.

The electrochemical impedance spectroscopy (EIS) of Mg-$CdTeO_3$ QDSSCs with different SILAR cycles and the corresponding fitting parameters are shown in Fig. 6 (left) and Table 4, respectively. The smaller the series resistance (R_s) is, the higher the fill factor can reach, and the lower R_{ct} is advantageous to electronic transmission; the greater electron recombination resistance (R_{rec}) is helpful to reduce the carrier recombination. Thus from comprehensive consideration, when the SILAR cycles are 2, the cell performance is the best. Therefore the J-V characteristic parameters are the best when the SILAR cycles are 2.

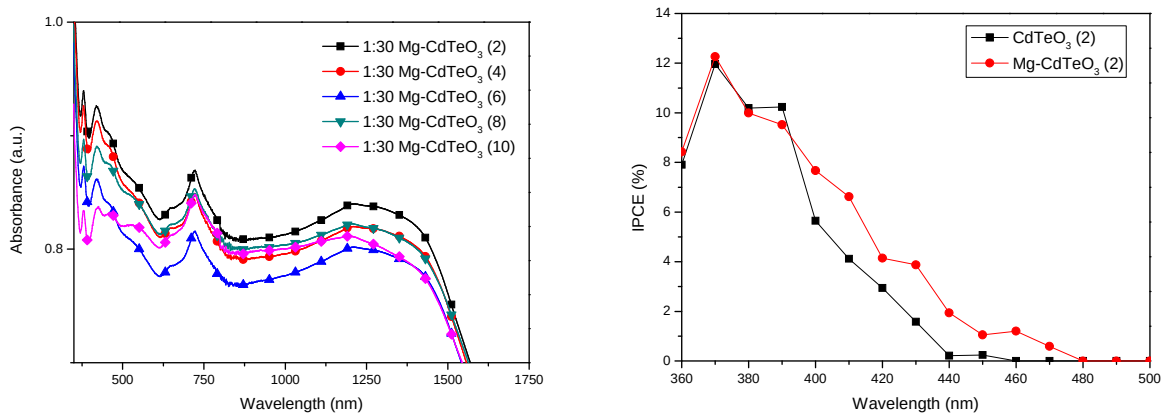

Fig. 7: UV-Vis absorption (right) and IPCE spectra (left) of Mg-doped-$CdTeO_3$ QDSSCs and undoped $CdTeO_3$ QDSSCs with two SILAR cycles

Based on above discussion, we can define the doped ratio of 1:30 as the most optimized doping concentration. Fig. 7 (right) gives the UV-Vis absorption spectra of Mg-$CdTeO_3$ QDs-sensitized NiO photocathode based on different SILAR cycles. As can be seen from the spectra, there are two small absorption peaks at around 400 nm and 700 nm. With the variation of SILAR cycles, the absorption spectra of photocathode show some subtle changes, and when SILAR cycles are 2, the absorption intensity is the highest. However, with the increase of SILAR cycles, the absorption intensity of photocathode is weakened gradually, but at a small degree. Obviously, the change rule of absorption spectrum is consistent with that of short-circuit current density.

The incident photon-to-electron conversion efficiency (IPCE) spectra of the Mg-doped-$CdTeO_3$ QDSSCs and $CdTeO_3$ QDSSCs with two SILAR cycles are shown in Fig. 7 (left), with a fixed doping ratio of 1:30. The maximum value (about 12%) appears around 370 nm. And the spectral response wavelength range of Mg-$CdTeO_3$ QDs-sensitized NiO photocathode is from 360 nm to 480 nm, which is, to some extent, wider than that of undoped photocathode. Moreover, this result can also be reflected through the short-circuit current density. Owing to the broaden spectral response range, the Jsc of Mg-doped-$CdTeO_3$ QDSSCs has a certain degree of improvement, compared with $CdTeO_3$ QDSSCs.

Conclusions

In summary, Mg doping has improved the performance of p-type NiO/$CdTeO_3$ QDSSCs. By contrast, the short-circuit current density (0.387 mA/cm^2) and power conversion efficiency (0.016 %) of Mg-$CdTeO_3$ QDSSCs are higher than that of undoped samples. Significantly, the Jsc is obviously enhanced, which is conducive to achieve the photocurrent matching of n-type solar cell and p-type solar cell, subsequently, to realize high theoretical power conversion efficiency of tandem solar cell.

Acknowledgments

This work was partially supported by Key Project of Beijing Natural Science Foundation (3131001), Key Project of Natural Science Foundation of China (91233201 and 61376057), State Key Laboratory of Solid State Microstructures of Nanjing University (M27019), State Key Laboratory for New Ceramic and Fine Processing of Tsinghua University (KF1210), Beijing Key Laboratory for Sensors of BISTU (KF20151077203, KF20151077204 and KF20151077205), and Beijing Key Laboratory for Photoelectrical Measurement of BISTU (GDKF2013005).

References

[1] M.Gratzel, Nature, 414 (2001), p. 338-344

[2] P. V. Kamat, K Tvrdy, D. R Baker, and Radich, J. G, Chem. Rev. Forum vol. 110 (2010), p. 6664-6688.

[3] I Mora-Sero, J Bisquert, J Phys. Chem. Lett. Forum vol. 1 (2010), p. 3046-3052

[4] A. J. Nozik, M. C. Beard, J. M. Luther, M. Law, R. J. Ellingson, and J. C. Johnson, Chem. Rev., Forum vol. 110 (2010), p. 6873-6890

[5] J. B. Sambur, T. Novet, and B. A. Parkinson, Science, Forum vol. 330 (2010), p. 63-66

[6] P. V. Kamat, J Phys. Chem., Forum vol. 112 (2008), p. 18737-18753

[7] J. Tang, Nature Materials, Forum vol. 10 (2011), p. 765-771

[8] Nattestad A. , Mozer A. J. , Fischer M. K. R. , et al. Natural materials, p. 31-35, 2010.

[9] A. Nattestad, A. J. Mozer, M. K. R. Fischer et al., Nature Materials, Forum vol. 9 (2010), p. 31-35

[10] J. H. Rhee, Y. H. Lee, P. Bera, and S. I. Seok, Forum vol. 477 (2009), p. 345-348

[11] F. Safari-Alamuti, J. R. Jennings, M. A. Hossain, L. Y. L. Yung, and Q. Wang, Physical Chemistry Chemical Physics, Forum vol. 15 (2013), p. 4767-4774

[12] Chuan Zhao, Xiaoping Zou, and Sheng He, Journal of Nanomaterials, Article ID 372381, 2014.

[13] A. Nattestad, A. J. Mozer, M. K. R. Fischer et al., Nature Materials, Forum vol. 9 (2010), p. 31-35

[14] L. Li, E. A. Gibson, P. Qin et al., Advanced Materials, Forum vol. 22 (2010), p. 1759-1762

[15] L. Li, E. A. Gibson, P. Qin et al., Advanced Materials, Forum vol. 22 (2010), p. 1759-1762

[16] S. He, X. Zou, Z. Sun, G. Teng, and C. Zhao, Journal of Materials Research, Forum vol. 28 (2013), p. 817-823